Vapor Condensation at the Free Surface of an Axisymmetric Liquid Mixed by a Laminar Jet

Chin-Shun Lin*
Analex Corporation, NASA Lewis Research Center, Cleveland, Ohio 44135

This paper presents numerical solutions of jet-induced mixing in a partially full cryogenic tank. An axisymmetric laminar jet is discharged from the central part of the tank bottom toward the liquid-vapor interface. Liquid is withdrawn at the same volume flow rate from the outer part of the tank. The jet is at a temperature lower than the interface, which is maintained at a certain saturation temperature. The interface is assumed to be flat and shear free and the condensation-induced velocity is assumed to be negligibly small compared with radial interface velocity. Finite-difference method is used to solve the nondimensional form of steady-state continuity, momentum, and energy equations. Calculations are conducted for jet Reynolds numbers ranging from 150 to 600 and Prandtl numbers ranging from 0.85 to 2.65. The effects of previously stated parameters on the condensation Nusselt and Stanton numbers that characterize the steady-state interface condensation process are investigated. Detailed analysis is performed to gain a better understanding of the fundamentals of fluid mixing and interface condensation.

Nomenclature

A_j	= surface area of central jet
A_{out}	= surface area of outflow at the tank bottom
A_s	= surface area of the liquid-vapor interface
B	= tank-to-jet diameter ratio, D/d
C_1, C_2, C_3, C_4	= constants
C_p	= specific heat at constant pressure
D	= tank diameter
d	= jet diameter
Fr	= Froude number, v_s^2/gD
g	= gravitational acceleration
h_c	= condensation heat transfer coefficient
h_{fg}	= latent heat of condensation
Ja_b	= bulk Jacob number, $C_p(T_s-T_{out})/h_{fg}$
Ja_j	= jet Jacob number, $C_p(T_s-T_j)/h_{fg}$
k	= thermal conductivity
m_c	= condensation mass flux
m, n	= constants of exponent in the correlation equations
Nu_c	= condensation Nusselt number, h_cD/k
p	= pressure
p_g	= equilibrium hydrostatic pressure
p^*	= dimensionless pressure, $(p-p_g)/\rho u_j^2$
Q	= jet volume flow rate
Re_j	= jet Reynolds number, $\rho u_j d/\mu$
r	= radial coordinate measured from the centerline
r^*	= dimensionless radial coordinate, r/D
St_c	= condensation Stanton number, $h_c/\rho u_j C_p$
T	= temperature
T_j	= jet temperature
T_s	= interface temperature
T_v	= vapor temperature
T^*	= dimensionless temperature, $(T-T_j)/(T_s-T_j)$
u	= axial velocity
u_c	= condensation-induced velocity
u_j	= jet velocity
u_{out}	= outflow velocity
u^*	= dimensionless axial velocity, u/u_j
u_c^*	= dimensionless condensation-induced velocity, u_c/u_j
v	= radial velocity
v_s	= radial velocity at the interface
v^*	= dimensionless radial velocity, v/u_j
v_s^*	= dimensionless radial velocity at interface
x	= axial coordinate measured from the tank bottom
x_p	= potential core length
x_s	= liquid filling height
x^*	= dimensionless axial coordinate, x/D
μ	= dynamic viscosity
ρ	= liquid density

Subscripts

b	= evaluated at bulk liquid
c	= evaluated at condensation condition
ct	= evaluated at tank centerline
j	= evaluated at jet inlet
out	= evaluated at outflow location
s	= evaluated at liquid-vapor interface
v	= evaluated at vapor region

Superscript

$-$	= average value over the interface

Introduction

THE thermal environment in space can result in radiation heat leak into the cryogen storage tanks and can increase the tank pressure. Of the various technologies[1] being developed for tank pressure control, axial jet-induced mixing[2] is considered an efficient method for a short-term storage system. The mixing of the tank contents causes a forced convection and removes heat quickly from the interface into the bulk liquid. The induced interface condensation then results in the reduction of tank pressure. It is obvious that the vapor condensation on the subcooled liquid at the interface plays a key role in reducing the tank pressure.

Several studies of steady-state fluid mixing and condensation rate have been conducted. Thomas[3] measured the condensation rate of steam on water surfaces mixed by a submerged jet. The liquid height-to-tank diameter ratio was varied from 0.32 to 1.3. It was found that the condensation rate was roughly proportional to the jet Reynolds number. Dominick[4] conducted experiments to investigate the effects of jet injec-

Received July 11, 1989; revision received Dec. 14, 1989; accepted for publication Dec. 22, 1989.

*Fluid Dynamics Scientist, Cryogenic Fluid Technology Office. Member AIAA.

tion angle and jet flow rate on the condensation rate in a Freon-113 tank. The ratio of liquid height to tank diameter was about 1. The tests showed that heat transfer at the interface was enhanced by the mixing process as the jet injection angle became more normal to the interface. The average heat transfer coefficient at the interface was found to be increasing with the jet Reynolds number to a power of 0.73. Sonin et al.[5] also measured the steady-state condensation rate of steam in a water tank with a liquid height-to-tank diameter ratio greater than 3. The condensation process was dominated by the liquid-side turbulence near the interface. About 0.3 of tank diameter below the interface, the turbulence was found isotropic and essentially unaffected by the proximity of the surface. A correlation between the condensation rate and characteristic interface turbulent velocity was also developed in Ref. 5. Hasan and Lin[6] used a finite-difference method to numerically solve time-averaged conservation equations along with a k-ϵ turbulence model for the prediction of turbulent velocity. Since the information about the turbulence at the interface was not available, zero gradients of k and ϵ were assumed for the boundary condition applied at the interface. The numerical prediction was in good agreement with Sonin's data except for the region close to the interface, where diffusion process was dominant. The failure of numerical solution for the near-interface region, as stated in Ref. 6, was probably due to the inappropriate turbulence model or the inappropriate turbulence boundary conditions applied at the interface.

For laminar flows, the fluid properties and boundary conditions are well defined. This motivates the present study to investigate more fundamentals of fluid mixing and the associated interface condensation process by a submerged laminar jet. For a typical cryogenic storage tank, the maximum liquid height-to-tank diameter ratio is about 1, and the mean-flow velocity is generally much larger than the turbulence at the interface. It is hoped that the study of laminar jet-induced mixing can provide some useful information for studying the turbulent jet-induced mixing in a typical cryogenic tank. In space the effect of buoyancy force may be insignificant due to the low-gravity environment. Therefore, the fluid mixing in low gravity may be equivalent to the mixing of constant-density liquid in normal gravity provided that the effect of free-surface configuration is excluded. The present study is conducted for a normal-gravity environment and neglects buoyancy force due to constant density. Numerical solutions are obtained by using a finite-difference method to solve nondimensional continuity, momentum, and energy equations. Calculations encompass a wide range of the Prandtl numbers and jet Reynolds numbers. Detailed analyses are performed, and simplified equations are generated to describe the effects of the preceding parameters on the condensation Nusselt and Stanton numbers that characterize the steady-state condensation process at the liquid-vapor interface.

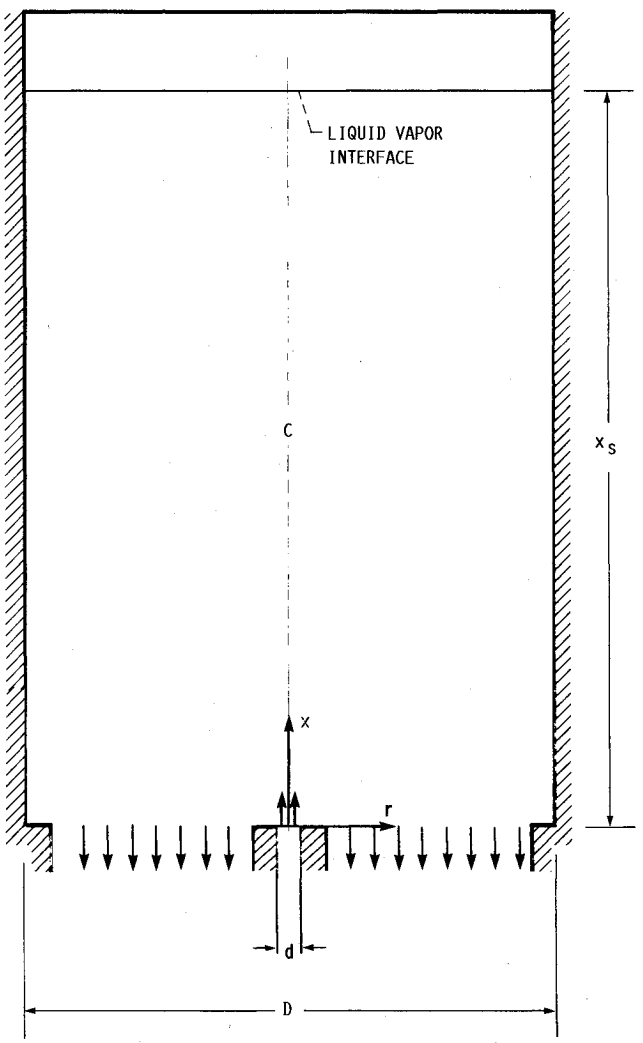

Fig. 1 Physical system and coordinates.

Physical Problem Considered

The physical system and the coordinates used to analyze the problem are shown in Fig. 1. A circular cylindrical tank of diameter D contains liquid with a filling height x_s. An axisymmetric laminar jet with a velocity u_j is discharged from the central part of the tank bottom toward the liquid-vapor interface. The liquid with the same volume flow rate Q is withdrawn from the outer part of the tank bottom so that the liquid fill level is kept constant. The outflow area A_{out} is much larger than inflow jet area A_j (about 357:1), so that the outflow velocity is very small compared with the jet velocity. Both the central jet and outflow velocities are assumed uniform. The ratio of d to D is fixed at 1:20. The ratio of x_s to D is set to 1.

The jet velocities are selected to be low enough so that the free surface is essentially flat (wave-free). The tank wall for vapor region is subjected to a low-radiation heat leak, and the increase of the vapor temperature will compensate for the pressure loss due to vapor condensation and then will maintain the tank at a constant pressure level. Therefore, the free surface can be kept at a constant saturation temperature T_s corresponding to the tank pressure. The superheat of the vapor is negligible compared with the liquid subcooling if both $(\rho_v/\rho_b)^{1/4}(\mu_v/\mu_b)^{1/2}$ and $C_{pv}(T_v - T_s)/h_{fg}$ are very small compared to 1 (Ref. 7), and the steady-state solution can be approximately applied to the liquid region for a limited time period. All of the solid walls are insulated. The central jet is kept at a constant temperature T_j, lower than the interface temperature. All of the associated thermodynamics and transport properties are assumed constant, since only a small temperature variation is considered in the whole flowfield. The outflow region is assumed to have a zero temperature gradient.

The energy balance at the interface yields the following relation between condensation mass flux and heat transfer:

$$\overline{m_c} h_{fg} A_s = \int m_c h_{fg}\, dA_s = \int \left(k \frac{\partial T}{\partial x}\right)_s dA_s \qquad (1)$$

where $\overline{m_c}$ and m_c are the average and local condensation mass fluxes at the interface, respectively. Experimentally, the steady-state condensation rate can be obtained based on the measurement of the temperature difference between outflow and inflow jet.[5] The relation of energy balance for the whole system yields

$$\overline{m_c} h_{fg} A_s = [\rho Q C_p (T_{out} - T_j)]/(1 + Ja_b) \qquad (2)$$

where T_{out} is the outflow temperature, which is essentially

uniform over the outflow area. Equations (1) and (2) can be used as a checkup of the numerical solutions. For commonly used cryogens such as hydrogen and nitrogen, Ja_b is usually much less than 1. For calculation convenience Ja_b is assumed to be zero in the present study. This assumption will be justified by the obtained solution later.

A local condensation heat transfer coefficient h_c and a local condensation Stanton number St_c, which describe the interfacial heat and mass transports, can be defined as

$$h_c = m_c h_{fg}/(T_s - T_j) \tag{3}$$

$$St_c = h_c/\rho u_j C_p \tag{4}$$

It is noted that, instead of the bulk liquid temperature and the interface velocity, the jet temperature and the jet velocity, respectively, are used in Eqs. (3) and (4). There are two reasons for these unusual definitions. First, the jet conditions are generally easy to control and measure so that the definitions in Eqs. (3) and (4) may be more useful. Second, the difference between bulk temperature and interface temperature is very small in the present study so that h_c will be very sensitive to the numerical error if $(T_s - T_b)$ is used in Eq. (3). For convenience, the average values of h_c and St_c at the interface are generally used in the analysis and are expressed as

$$\overline{h_c} = \overline{m_c} h_{fg}/(T_s - T_j) \tag{5}$$

$$\overline{St_c} = \overline{h_c}/\rho u_j C_p \tag{6}$$

Mathematical Formulation

The jet-induced mixing considered in the present study is steady state and incompressible with gravity acting in the vertical $-x$ direction. The governing equations for this axisymmetric laminar flow problem are

$$\frac{\partial}{\partial x}(u) + \frac{\partial}{r\partial r}(rv) = 0$$

$$\frac{\partial}{\partial x}(u^2) + \frac{\partial}{r\partial r}(urv) = -\frac{1}{\rho}\frac{\partial p}{\partial x} - g + \frac{\mu}{\rho}\frac{\partial^2 u}{\partial x^2} + \frac{\mu}{\rho}\frac{\partial}{r\partial r}\left(r\frac{\partial u}{\partial r}\right)$$

$$\frac{\partial}{\partial x}(uv) + \frac{\partial}{r\partial r}(rv^2) = -\frac{1}{\rho}\frac{\partial p}{\partial r} - \frac{\mu}{\rho}\frac{v}{r^2} + \frac{\mu}{\rho}\frac{\partial^2 v}{\partial x^2} + \frac{\mu}{\rho}\frac{\partial}{r\partial r}\left(r\frac{\partial v}{\partial r}\right)$$

$$\frac{\partial}{\partial x}(uT) + \frac{\partial}{r\partial r}(vrT) = \frac{k}{\rho C_p}\frac{\partial^2 T}{\partial x^2} + \frac{k}{\rho C_p}\frac{\partial}{r\partial r}\left(r\frac{\partial T}{\partial r}\right)$$

The boundary conditions are applied for the system sketched in Fig.1. At the centerline, the symmetric conditions are used:

$$v = 0, \qquad \frac{\partial u}{\partial r} = \frac{\partial T}{\partial r} = 0$$

At the solid walls, the nonslip and adiabatic conditions are employed:

$$u = v = 0, \qquad \frac{\partial T}{\partial x} = \frac{\partial T}{\partial r} = 0$$

Free-surface waviness is always present to some degree. In the present calculations the Froude number, defined as $Fr = v_s^2/gD$, will be shown to be much less than 1 so that the surface is approximately flat. The vapor viscosity is much less than the liquid viscosity, and the shear-free condition applies. The condensation-induced velocity at the interface u_c is equal to

$$u_c = m_c/\rho \tag{7}$$

and is assumed negligible compared with surface velocity. This assumption will also be justified by the obtained numerical solutions. Thus, the free-surface boundary conditions for velocity are approximated by

$$u = 0, \qquad \frac{\partial v}{\partial x} = 0$$

The neglecting of u_c leads to the uncoupling between fluid dynamics and thermal calculations. The temperature of the interface is kept constant at T_s. For the jet inlet, the velocity and temperature are assumed to be uniform:

$$u = u_j, \qquad v = 0, \qquad T = T_j$$

Liquid is withdrawn from the outer part of the tank bottom with the same volume flow rate as that of the injected liquid jet, so that the uniform withdrawing velocity can be obtained by Q/A_{out}. The conditions for radial velocity and temperature applied at this liquid-withdrawing plane are given by

$$v = 0, \qquad \frac{\partial T}{\partial x} = 0$$

Nondimensionalized variables can be formed as

$$x^* = \frac{x}{D}, \qquad r^* = \frac{r}{D}, \qquad u^* = \frac{u}{u_j}, \qquad v^* = \frac{v}{u_j},$$

$$p^* = \frac{p - p_g}{\rho u_j^2}, \qquad T^* = \frac{T - T_j}{T_s - T_j}$$

where, for convenience, the gravity term has been subtracted from the x-momentum equation by using the static equilibrium equation:

$$\frac{\partial p_g}{\partial x} = -\rho g$$

The dimensionless forms of the steady-state governing equations are

$$\frac{\partial u^*}{\partial x^*} + \frac{\partial r^* v^*}{r^* \partial r^*} = 0$$

$$\frac{\partial u^{*2}}{\partial x^*} + \frac{\partial u^* r^* v^*}{r^* \partial r^*} = -\frac{\partial p^*}{\partial x^*} + \frac{1}{BRe_j}\left[\frac{\partial^2 u^*}{\partial x^{*2}} + \frac{\partial}{r^* \partial r^*}\left(r^*\frac{\partial u^*}{\partial r^*}\right)\right]$$

$$\frac{\partial u^* v^*}{\partial x^*} + \frac{\partial r^* v^{*2}}{r^* \partial r^*} = -\frac{\partial p^*}{\partial r^*} - \frac{1}{BRe_j}\frac{v^*}{r^{*2}} + \frac{1}{BRe_j}\left[\frac{\partial^2 v^*}{\partial x^{*2}} + \frac{\partial}{r^* \partial r^*}\left(r^*\frac{\partial v^*}{\partial r^*}\right)\right]$$

$$\frac{\partial u^* T^*}{\partial x^*} + \frac{\partial r^* v^* T^*}{r^* \partial r^*} = \frac{1}{BRe_j Pr}\left[\frac{\partial^2 T^*}{\partial x^{*2}} + \frac{\partial}{r^* \partial r^*}\left(r^*\frac{\partial T^*}{\partial r^*}\right)\right]$$

The relevant parameters in the governing equations are Re_j, Pr, and the tank-to-jet diameter ratio B:

$$Re_j = \rho u_j d/\mu, \qquad Pr = C_p \mu/k, \qquad B = D/d$$

The average condensation Nusselt number at the interface $\overline{Nu_c}$ is defined by

$$\overline{Nu_c} = \overline{h_c} D/k$$

From Eqs. (5) and (6) the average condensation Nusselt number and Stanton number can then be expressed as

$$\overline{Nu_c} = 8\int\left(\frac{\partial T^*}{\partial x^*}\right)_s r^*\,dr^* \tag{8}$$

$$\overline{St_c} = \overline{Nu_c}/BRe_jPr \tag{9}$$

The corresponding boundary conditions are then as follows.

At the centerline (symmetric conditions),

$$v^* = 0, \qquad \frac{\partial u^*}{\partial r^*} = \frac{\partial T^*}{\partial r^*} = 0$$

At the solid walls (nonslip and adiabatic conditions),

$$u^* = v^* = 0, \qquad \frac{\partial T^*}{\partial x^*} = \frac{\partial T^*}{\partial r^*} = 0$$

At the interface,

$$u^* = 0, \qquad \frac{\partial v^*}{\partial x^*} = 0, \qquad T^* = 1$$

At the jet inlet,

$$u^* = 1, \qquad v^* = 0, \qquad T^* = 0$$

At liquid-withdrawn plane,

$$u^* = \frac{-Q}{u_j A_{\text{out}}}, \qquad v^* = 0, \qquad \frac{\partial T^*}{\partial x^*} = 0$$

The effects of Re_j on the dynamics of fluid mixing in the tank and the steady-state condensation rate at the liquid-vapor interface are investigated. Calculations will be performed with Re_j ranging from 150 to 600 in which the flow is expected to be laminar according to the experiments of McNaughton and Sinclair.[8] The Pr will be varied from 0.85 to 2.65 to represent various cryogens such as hydrogen and nitrogen so that the performance of fluid mixing can be evaluated.

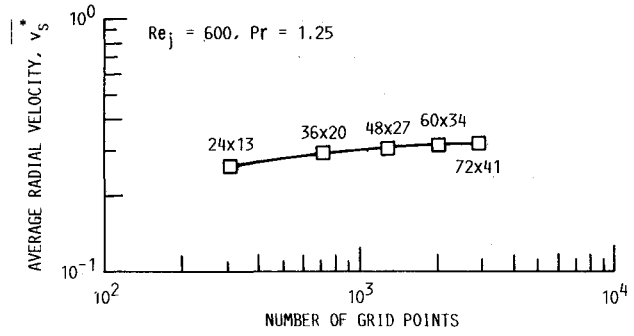

Fig. 2 Effect of grid size on the average radial velocity at the interface.

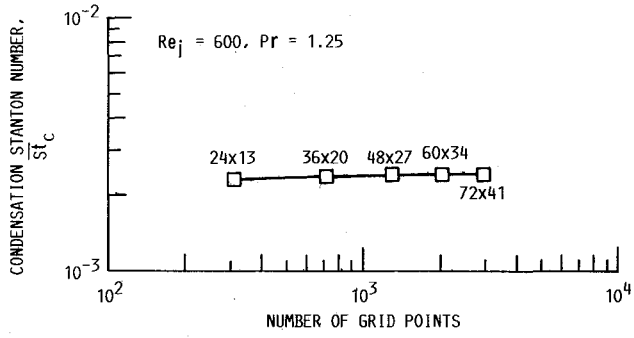

Fig. 3 Effect of grid size on the average condensation Stanton number.

Numerical Method of Solutions

The dimensionless forms of elliptic partial differential equations are numerically solved by a finite-difference method. The finite-difference equations are derived by integrating the differential equations over an elementary control volume surrounding a grid node appropriate for each dependent variable.[9] A staggered grid system is used so that the scalar properties, p and T, are stored midway between the u and v velocity grid nodes. The bounded skew hybrid differencing (BSHD) is incorporated for the convective terms,[9] and the integrated source terms are linearized. Pressures are obtained from a predictor-corrector procedure of the pressure implicit split operator (PISO) method,[10] which yields the pressure change needed to procure velocity changes to satisfy mass continuity. The governing finite-difference equations are solved iteratively by the ADI method with under-relaxation until the solutions are converged.

Calculations are performed with a nonuniform grid distribution with concentration of the grid nodes in the centerline, near-wall, and near-interface regions where the gradients of flow properties are expected to be large. The nonuniform grid distribution in axial direction is generated by using an exponential function of Roberts' transformation[11] with a stretching parameter equal to 1.02. In the radial direction the scheme[12] with a constant ratio between two adjacent grid spacing is used. This ratio is set to be about 1.22 in the present study. To check grid dependency, the cases with 24 × 13, 36 × 20, 48 × 27, 60 × 34, and 72 × 41 nodes are run for $Re_j = 600$ and $Pr = 1.25$. Figures 2 and 3 show that there is little change in $\overline{v_s^*}$ and $\overline{St_c}$, respectively, between grid distributions 60 × 34 and 72 × 41. It is then decided to use 72 × 41 grid nodes for all of the calculations in the present study. Calculations are performed on a Cray XMP computer located at NASA Lewis Research Center. The convergent solutions are considered to be reached when the absolute value of [Eq. (2) − Eq. (1)]/Eq. (1) is less than 0.003 and the maximum of absolute residual sums for each dependent variable is less than 10^{-6}.

Results and Analysis

A potential core length x_p is defined as the distance between the jet exit and the point where the jet centerline velocity begins to decrease. As shown in Fig. 4, the potential core length is linearly increasing with jet Reynolds number and can be described by the following equation:

$$x_p/d = C_1 Re_j$$

where C_1 is 0.0067 for the tankage considered in the present study. The conclusion of a linear relation between potential core length and jet Reynolds number is in agreement with the analysis of free jet in Ref. 13. The centerline velocity u_{ct}^* decays slowly approaching the liquid-vapor interface. The

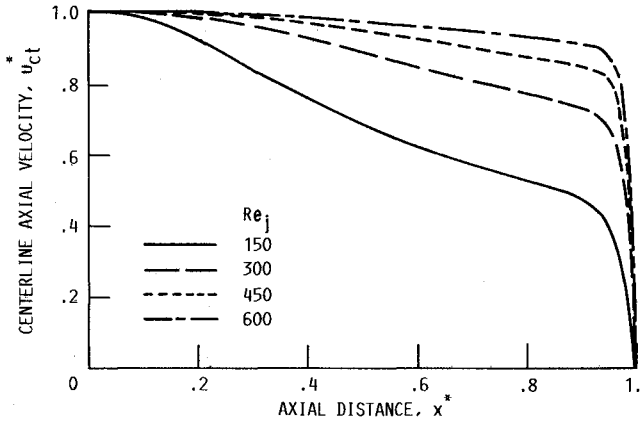

Fig. 4 Distribution of dimensionless axial velocity along the centerline.

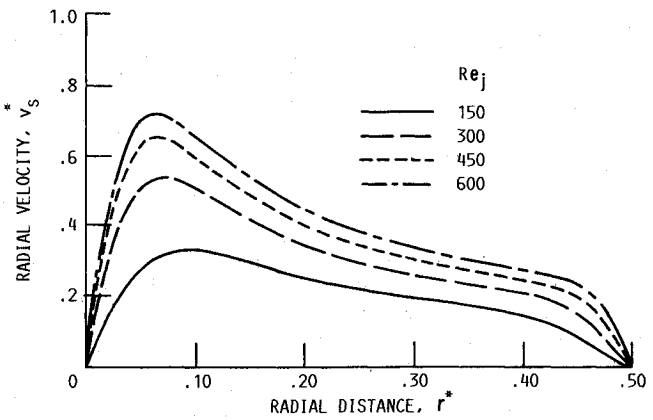

Fig. 5 Distribution of dimensionless radial velocity at the interface.

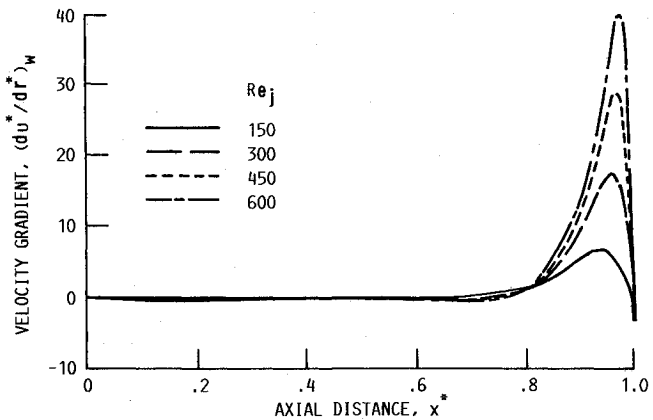

Fig. 6 Distribution of dimensionless axial velocity gradient along the tank side wall.

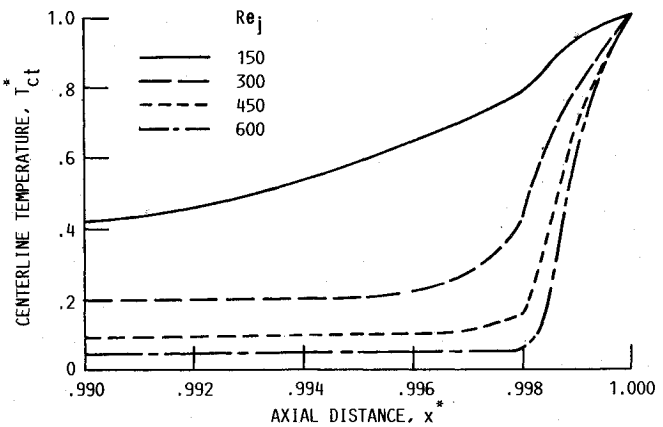

Fig. 7 Distribution of dimensionless temperature along the centerline for $Pr = 1.25$.

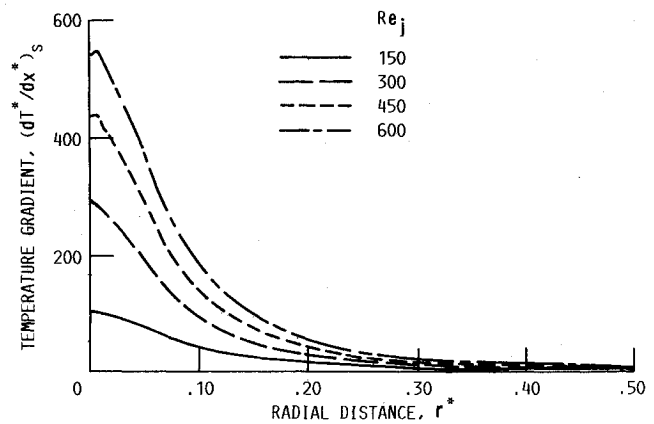

Fig. 8 Radial distribution of dimensionless temperature gradient at the interface for $Pr = 1.25$.

velocity drops to zero abruptly at the interface with greater decreasing rate for a higher jet Reynolds number. The upstream effect of the existence of the interface is less for higher jet Reynolds numbers. Figure 4 also indicates that a flat surface assumption may be more adequate at smaller jet Reynolds numbers. It is noted that both the potential core length and the decaying rate of centerline velocity are less than those in Ref. 13 because of the difference between the two physical flow systems considered, resulting in different values of C_1. As the jet approaches the interface, an impingement region is created just underneath the interface. This region plays the most important role in the bulk-mixing process since the flow in this region removes the heat from the interface into the bulk liquid and induces the vapor condensation. The radial distribution of the free-surface velocity v^* is shown in Fig. 5. The v_s^* increases from zero at the centerline to reach a peak shortly and then decreases approaching the side wall. For a higher jet Reynolds number this peak velocity is larger and is located closer to the centerline. As expected, the average dimensionless surface velocity $\bar{v}_s^*$ is increasing with Re_j and is approximately proportional to $Re_j^{1/2}$:

$$\bar{v}_s^* = \bar{v}_s/u_j = C_2 Re_j^{1/2}$$

where C_2 is 0.0134 in the present study. Consequently, the average interface radial velocity is approximately increasing with $u_j^{3/2}$. The Froude number based on $\bar{v}_s$ can be expressed as

$$Fr = \bar{v}_s^2/gD = (C_2\mu/\rho)^2 Re_j^3 B^2/gD^3$$

For liquid hydrogen, nitrogen, or oxygen with $Re_j = 600$ and $B = 20$, the Froude number is on the order of $0.000001/(gD^3)$ (in International System units), which is easily much less than 1 for a normal-gravity condition. Therefore, the flat free-surface assumption is acceptable in the present calculations. For a low-gravity condition the tank needs to be large enough in order to have $Fr \ll 1$.

The existence of liquid-vapor interface and tank side walls and the withdrawing of the liquid from the outer part of the tank bottom enhance the flow circulation in the tank. Figure 6 shows the velocity gradient distribution at the side wall resulting from the liquid flowing toward the tank bottom. Because the backward axial velocity is very small, the wall shear is negligible at most of the tank side walls except the region near the interface. The value of the maximum wall shear is higher and is located closer to the interface for jets with higher Reynolds number. The distance of the location of maximum wall shear from the interface is observed to be approximately the same as the thickness of the impingement region. From Fig. 6 the radial boundary-layer thickness appears to reach a value of about $0.025D$ (i.e., a value of about $0.5\,d$) as the jet Reynolds number is increased. This finding is in agreement with that for a turbulent jet in Ref. 2.

For $Pr = 1.25$ the axial temperature distribution at the centerline, $r = 0$, as a function of jet Reynolds number is shown in Fig. 7. The centerline temperature increases slowly approaching the interface with higher increasing rate for a smaller jet Reynolds number. Consequently, in the region near the interface, higher jet Reynolds numbers yield much higher temperature gradients to approach the interface temperature. The radial distribution of temperature gradient at the interface is given in Fig. 8. As observed, a high jet Reynolds number flow induces more interface condensation. Most of the mass condensation occurs in the central part of the interface for the ratio of jet diameter to tank diameter equal to 0.05 considered in the present study. It is expected that, if the jet nozzle to tank diameter ratio is small enough, the difference of interface configuration between low gravity and normal gravity will not have a significant effect on the interface condensation. There-

fore, as mentioned in the Introduction, the fluid mixing processes of low gravity and normal gravity may be equivalent if the buoyancy force is neglected and the free-surface condition is not enormously different from that assumed in the present study. Calculations were also performed for Prandtl numbers that varied from 0.85 to 2.65 with various jet Reynolds numbers. The effect of the Prandtl number on the distributions of centerline temperature and interface temperature gradient was found to be similar to that of the jet Reynolds number, as shown in Figs. 7 and 8. A higher Prandtl number will yield a larger condensation heat flux over the interface and a thinner thickness of thermal layer underneath the interface. It is noted that, for higher jet Reynolds numbers and Prandtl numbers, the maximum of temperature gradient at the interface is slightly shifted away from the centerline due to the effect of significant surface motion. The radial distribution of temperature at $x^* = 0.97$ is shown in Fig. 9. The higher jet Reynolds number yields lower flow temperature in the central jet region, approaching bulk liquid temperature with higher increasing rate at the edge of jet region, and results in a thinner thermal layer underneath the interface.

The u_c^* can be calculated by

$$u_c^* = \frac{u_c}{u_j} = \frac{(\partial T^*/\partial x^*)_s Ja_j}{PrRe_jB}$$

where the jet Jacob number is defined as $C_p(T_s - T_j)/h_{fg}$. The maximum of u_c^* is located at the centerline. For liquid hydrogen at a saturation pressure of 30 psia with 2°R of jet subcooling, the maximum values of u_c^* for $Re_j = 600$ and 150 are equal to 0.0011 and 0.0009, respectively. From Fig. 5 it is observed that u_c^* is negligible compared with surface velocity v_s^* except for the very small stagnation region. The temperature difference between the bulk liquid and the interface is much smaller than that between the jet and the interface. For $(T_s - T_j)$ equal to 2°R, $(T_s - T_{out})$ is approximately equal to 0.06°R, and the corresponding Ja_b is equal to 0.001. It can then be justified that the assumption of neglecting u_c and Ja_b in the present study is acceptable.

The correlation for the average condensation Nusselt number is assumed to be of the form

$$\overline{Nu_c} = C_3 Re_j^m Pr^n \tag{10}$$

Based on the obtained numerical solution, the values of C_3, m, and n are approximately equal to 0.049, 1.0, and 0.97, respectively. As shown in Figs. 10 and 11, the average condensation Nusselt number is linearly proportional to the jet Reynolds number and is nearly a linear function of Prandtl number. It is noted that the constant n is actually a weak function of Prandtl number itself and is decreasing from 1.0 for $Pr = 0.85$ to 0.95 for $Pr = 2.65$. The value of n is expected to slightly decrease as the Prandtl number keeps increasing. Equation (10) also implies that the condensation mass flux is linearly increasing with jet Reynolds number, which is in agreement with the data for turbulent jet in Ref. 3. From Eqs. (9) and (10) the correlation for average condensation Stanton number can be expressed as

$$\overline{St_c} = C_4 Pr^{n-1} = C_4 Pr^{-0.03} \tag{11}$$

where C_4 is equal to 0.00245. The average condensation Stanton number is a weak function of Prandtl number only and is independent of jet Reynolds number. In the present study only the jet Reynolds number and the Prandtl number are investigated, and the other relevant tankage system parameters such as $B(= D/d)$, x_s/D, and A_{out}/A_j are specified. Therefore, it is expected that the correlation constants C_1, C_2, C_3, and C_4 obtained from the preceding analysis need to be modified if a different tankage system is considered.

From Eqs. (2), (5), and (6) the average condensation Stanton number for $Ja_b = 0$ can be expressed as

$$\overline{St_c} = [(T_{out} - T_j)/(T_s - T_j)](d/D)^2 \tag{12}$$

If the outflow temperature T_{out} approaches T_s, Eq. (12) will become

$$\overline{St_c} \approx (d/D)^2 \tag{13}$$

Equation (13) implies that $\overline{St_c}$ is nearly a constant and is simply determined by system geometry, provided that the flow conditions can yield T_{out} close to T_s. The physical phenomenon behind Eq. (13) is that the cold jet simply enters, sweeps by the interface, and receives as much heat as it can absorb, reaching saturation temperature and exiting. Equation (13) gives an upper bound for $\overline{St_c}$ based on an energy balance with the outflow liquid at its maximum possible temperature. In the present computation $d/D = 1/20$, and Eq. (13) gives

$$\overline{St_c} = 0.0025 \tag{14}$$

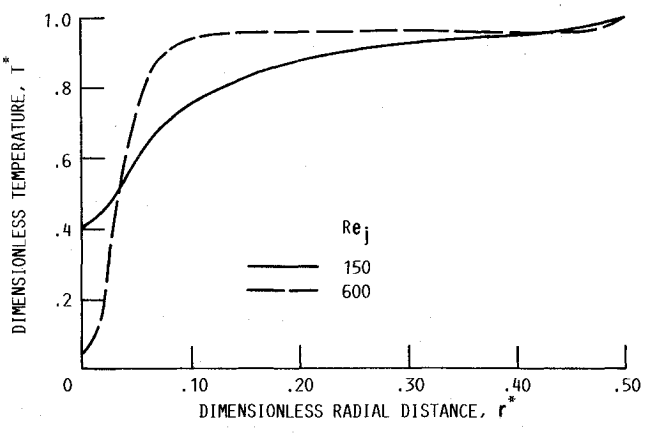

Fig. 9 Radial distribution of temperature at $x^* = 0.97$ as a function of jet Reynolds number for $Pr = 1.25$.

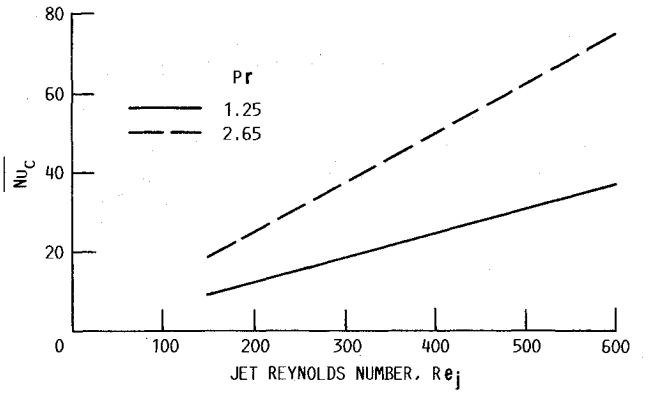

Fig. 10 Average condensation Nusselt number as a function of jet Reynolds number.

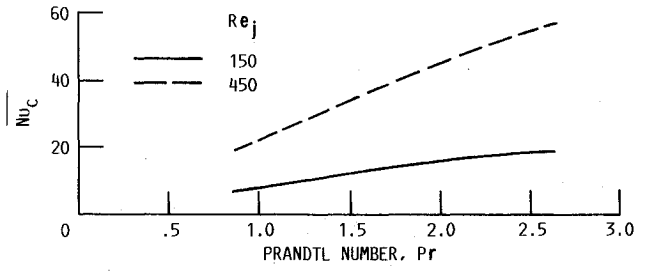

Fig. 11 Average condensation Nusselt number as function of Prandtl number.

which is in excellent agreement with the numerical correlation shown in Eq. (11). It can be concluded that, for laminar operating conditions with a jet Reynolds number up to 600, the injected liquid reaches essentially interface saturation temperature before exiting (at least for a tankage system of $d/D = 1/20$), and the total condensation rate is controlled by the jet volume flow rate rather than by the condensation heat transfer coefficient at the interface.

Conclusions

The nondimensional form of steady-state continuity, momentum, and energy equations has been solved by a finite-difference method. Numerical solutions were obtained for a laminar jet-induced fluid mixing in a cryogenic tank system shown in Fig. 1. The temperature variation in the whole flowfield was small so that the thermodynamics and transport properties were assumed constant. The effect of buoyancy force was neglected. The interface was assumed to be flat (wave-free) and shear-free. The condensation-induced velocity at the interface and the associated bulk and jet Jacob numbers were assumed to be zero. Calculations were performed for jet Reynolds numbers ranging from 150 to 600 and Prandtl numbers ranging from 0.85 to 2.65. Based on the tankage system considered in the present study, the following conclusions have been drawn:

1) The ratio of average radial interface velocity to jet velocity is approximately proportional to $Re_j^{1/2}$, and the average interface radial velocity is approximately proportional to $u_j^{3/2}$. The thickness of the impingement region layer underneath the interface is decreasing with increasing jet Reynolds number and appears to approach a value of one-half of the jet diameter as jet Reynolds number is further increased.

2) The condensation Nusselt number and then the condensation mass flux are linearly increasing with jet Reynolds number. The condensation Stanton number is independent of jet Reynolds number and is proportional to Pr^{1-n} with n approximately equal to 0.97 for Prandtl numbers ranging from 0.85 to 2.65. The value of the exponent n is slightly decreasing with increasing Prandtl number. The thermal-layer thickness underneath the interface is thinner for higher values of jet Reynolds number and Prandtl number.

3) For laminar operating conditions with a jet Reynolds number ranging from 150 to 600, the injected liquid reaches essentially interface saturation temperature before exiting (at least for a tankage system with $x_s/D = 1$ and $d/D = 1/20$), and the interface condensation rate is jet volume flow limited.

4) If the ratio of jet nozzle to tank diameter is small enough, most of the vapor condensation will occur at the central part of the interface, and the effect of the difference of interface configuration between low gravity and normal gravity on the interface condensation may be insignificant. The present calculations suggest that the condensation may be expected to be volume flow limited also in the low gravity case provided the free surface is not enormously different from the one assumed in the present study.

References

[1]Aydelott, J. C., Carney, M. J., and Hochstein, J. I., "NASA Lewis Research Center Low-Gravity Fluid Management Technology Program," NASA TM-87145, 1985.

[2]Poth, L. J., and Van Hook, J. R., "Control of the Thermodynamic State of Space-Stored Cryogens by Jet Mixing," *Journal of Spacecraft and Rockets,* Vol. 9, No. 5, 1972, pp. 332–336.

[3]Thomas, R. M., "Condensation of Steam on Water in Turbulent Motion," *International Journal of Multiphase Flow,* Vol. 5, No. 1, 1979, pp. 1–15.

[4]Dominick, S. M., "Mixing Induced Condensation Inside Propellant Tanks," AIAA Paper 84-0514, Jan. 1984.

[5]Sonin, A. A., Shimko, M. A., and Chun, J. H., "Vapor Condensation onto a Turbulent Liquid—I. The Steady Condensation Rate as a Function of Liquid-Side Turbulence," *International Journal of Heat Mass Transfer,* Vol. 29, No. 9, 1986, pp. 1319–1332.

[6]Hasan, M. M., and Lin, C.-S., "Axisymmetric Confined Turbulent Jet Directed Towards the Liquid Surface From Below," AIAA Paper 89-0172, Jan. 1989; also NASA TM-101409.

[7]Gerner, F. M., and Tien, C. L., "Axisymmetric Interfacial Condensation Model," *ASME Proceedings of the 1988 National Heat Transfer Conference,* Vol. 3, American Society of Mechanical Engineers, New York, Publ. HTD-96, 1988, pp. 235–242.

[8]McNaughton, K. J., and Sinclair, C. G., "Submerged Jets in Short Cylindrical Flow Vessels," *Journal of Fluid Mechanics,* Vol. 25, Pt. 2, June 1966, pp. 367–375.

[9]Syed, S. A., Chiappetta, L. M., and Gosman, A. D., "Error Reduction Program," Pratt & Whitney Aircraft Co., East Hartford, CT, Rept. PWA-5928-25, 1985; also NASA CR-174776.

[10]Issa, R. I., "Solution of the Implicitly Discretised Fluid Flow Equations by Operator-Splitting," *Journal of Computational Physics,* Vol. 62, No. 1, 1986, pp. 40–65.

[11]Roberts, G. O., "Computational Meshes for Boundary Layer Problems," *Proceedings of the Second International Conference on Numerical Methods in Fluid Dynamics,* Vol. 8, edited by M. Holtz, Springer-Verlag, New York, 1971, pp. 171–177 (*Lecture Notes in Physics*).

[12]Cebeci, T., and Smith, A. M. O., *Analysis of Turbulent Boundary Layers,* Academic, New York, 1974.

[13]Gauntner, J. W., Livingood, J. N. B., and Hrycak, P., "Survey of Literature on Flow Characteristics of a Single Turbulent Jet Impinging on a Flat Plate," NASA TN D-5652, Feb. 1970.